




Research Article

CdS/Bi₁₂O₁₇Cl₂ Heterostructure Promotes Visible-Light-Driven Photocatalytic CH₄ Generation and Phenol Conversion

Dandan Hu,¹ Yumin Cui,¹ Xiaoyan Cao,¹ Yan Han,¹ Huiquan Li ,¹ Hui Miao ,¹ Yuying Wu,¹ Huidan Yang,¹ Wei Zhao,¹ Chaonan Xu,¹ and Yupeng Yuan ²

¹Anhui Provincial Key Laboratory for Degradation and Monitoring of Pollution of the Environment, School of Chemistry and Materials Engineering, Fuyang Normal University, Fuyang 236037, China

²School of Chemistry and Chemical Engineering, Anhui University, Hefei 230601, China

Correspondence should be addressed to Huiquan Li; huiquanli0908@163.com, Hui Miao; huimiao@ahnu.edu.cn, and Yupeng Yuan; yupengyuan@ahu.edu.cn

Received 10 July 2021; Revised 19 November 2021; Accepted 7 December 2021; Published 22 January 2022

Academic Editor: Adel A. Ismail

Copyright © 2022 Dandan Hu et al. This is an open access article distributed under the Creative Commons Attribution License, which permits unrestricted use, distribution, and reproduction in any medium, provided the original work is properly cited.

We report a heterojunction photocatalyst by coupling CdS with Bi₁₂O₁₇Cl₂ via a facile thermal annealing process. Such heterostructure can promote the charge separation between CdS and Bi₁₂O₁₇Cl₂, thereby leading to a considerable improvement on the performance for CO₂ reduction into valuable CH₄ and phenol conversion under visible light exposure. The CdS/Bi₁₂O₁₇Cl₂ heterojunction with mass ratio of 1:1 (50% CdS/Bi₁₂O₁₇Cl₂) shows the highest CH₄ production rate (1.28 μmol·h⁻¹·g⁻¹), which is as 9.8 and 5.8 times as the CH₄ generation rate of pure Bi₁₂O₁₇Cl₂ and CdS (0.13 and 0.22 μmol·h⁻¹·g⁻¹), respectively. Also, the 50% CdS/Bi₁₂O₁₇Cl₂ sample shows the highest activity of phenol conversion with a conversion ratio of 92%, which is as 2.2 times and 1.9 times as the conversion ratio of pristine Bi₁₂O₁₇Cl₂ (41%) and CdS (48%), respectively. The present study demonstrates the great potential of the CdS/Bi₁₂O₁₇Cl₂ heterojunction for efficient charge separation towards increased photocatalytic CH₄ production and phenol conversion.

1. Introduction

Nowadays, photocatalytic technology has garnered numerous attentions for solar fuel production and environmental purification [1–5]. After decades of studies, hundreds of photocatalysts have been reported on hydrogen generation [6, 7], CO₂ reduction [8–11], NO removal [12], and organic pollutant degradation [13, 14]. Bismuth oxychlorides refer to compounds with different ratios of Bi:O:Cl (e.g., BiOCl, Bi₃O₄Cl, Bi₁₂O₁₇Cl₂, and Bi₂₄O₃₁Cl₁₀) [15–18], which has become one of the research hotspots of photocatalytic applications in recent years. Among these compounds, Bi₁₂O₁₇Cl₂ photocatalyst has aroused great interest of scientists due to its excellent visible light absorption capacity, strong oxidation capacity, and small bandgap energy [19–22]. Zhang et al. prepared a two-dimensional BiOCl/Bi₁₂O₁₇Cl₂ heterojunction photocatalyst, which improved the photocatalytic removal efficiency of nitric oxide (NO)

[23]. Ma et al. prepared a new two-dimensional layered MoS₂/Bi₁₂O₁₇Cl₂ photocatalyst, which increased the visible light absorption range and accelerated the degradation rate of Rhodamine B (RhB) [24]. He et al. synthesized a novel three-dimensional flower-like Bi₁₂O₁₇Cl₂/β-Bi₂O₃, which enhanced the photocatalytic activity of 4-tert-butyl phenol under visible light irradiation [25]. Thus, the photocatalytic performance of Bi₁₂O₁₇Cl₂ can be effectively improved by forming heterojunction structure with other semiconductors.

CdS is narrow bandgap semiconductor with strong visible light capture capability, which can be used in photocatalytic CO₂ reduction, hydrogen generation, and pollutant degradation [26–30]. However, the application of CdS is limited by photocorrosion and rapid recombination of photogenerated electron-hole pairs [31, 32]. Studies have shown that the construction of heterojunction photocatalysts can effectively separate photocarriers and significantly

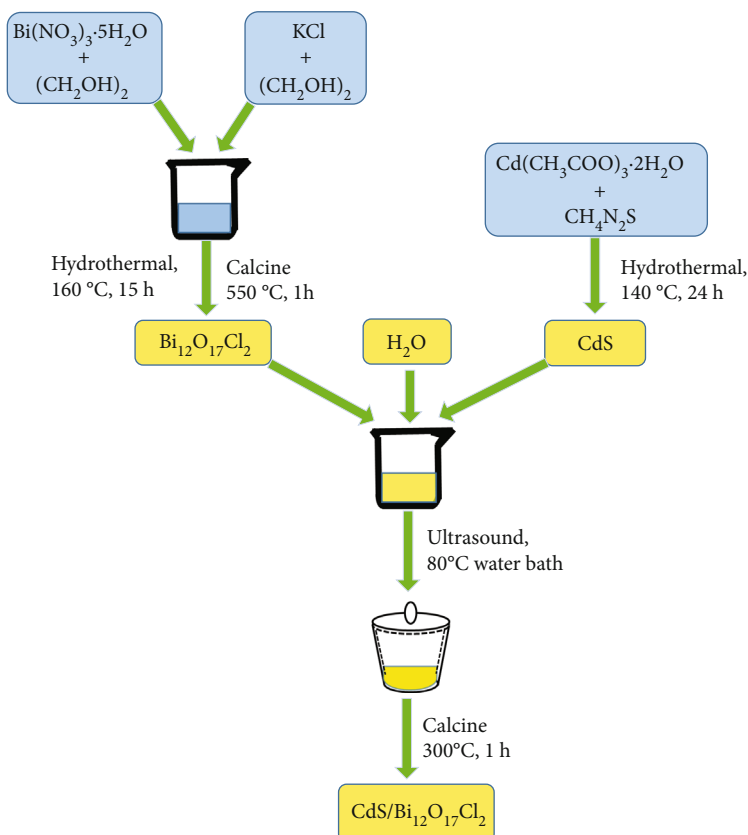


FIGURE 1: The preparation flow chart of CdS/Bi₁₂O₁₇Cl₂ heterojunctions.

improve the photocatalytic performance; the multicomponent photocatalysts made of different semiconductors become a feasible method to improve the photocatalytic efficiency [33–36]. Herein, we report on the fabrication of a visible-light-driven CdS/Bi₁₂O₁₇Cl₂ heterostructure for both CO₂ reduction and phenol conversion. The results showed that CdS/Bi₁₂O₁₇Cl₂ heterojunction could effectively improve the photocatalytic reduction rate of carbon dioxide and the removal ratio of phenol.

2. Experiments

2.1. Synthesis of Catalysts. Bi₁₂O₁₇Cl₂ samples were prepared by a hydrothermal method [37]. In this preparation method, Bi(NO₃)₃·5H₂O (9 mmol) and KCl (1.5 mmol) were dissolved in an appropriate amount of ethylene glycol, respectively. Add the KCl solution to the bismuth nitrate solution slowly. The compound was stirred for 0.5 h and then kept 160 °C for 15 h in a Teflon-lined stainless-steel autoclave (100 mL). The acquired precipitation was collected, washed, and dried. And the powder was further heated at 550 °C for 1 h in a muff furnace. Finally, the product was ground to yield the yellow Bi₁₂O₁₇Cl₂.

In a typical synthesis of CdS [38], cadmium acetate dihydrate (6.4 mmol) and thiourea (32 mmol) were first added to deionized water (70 mL) under magnetic stirring for 0.5 h. The compound was then kept 140 °C for 24 h in a Teflon-lined stainless-steel autoclave (100 mL). And the product

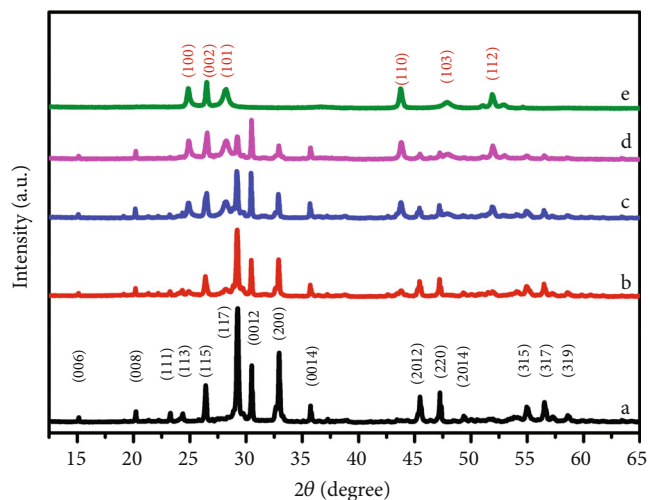


FIGURE 2: XRD patterns of Bi₁₂O₁₇Cl₂ (a), 34% CdS/Bi₁₂O₁₇Cl₂ (b), 50% CdS/Bi₁₂O₁₇Cl₂ (c), 60% CdS/Bi₁₂O₁₇Cl₂ (d), and CdS (e).

was collected, washed, and dried to obtain the orange powder.

To prepare the CdS/Bi₁₂O₁₇Cl₂ heterojunction catalyst, Bi₁₂O₁₇Cl₂ (0.3 mmol) and a certain amount of CdS thus obtained were first mixed in 30 mL deionized water under the ultrasonic treatment for 1 h and then dried in a water bath at 80 °C. And the mixture was heated at 300 °C for 1 h to gain the CdS/Bi₁₂O₁₇Cl₂ sample. The complete process of heterojunction preparation is shown in Figure 1. By

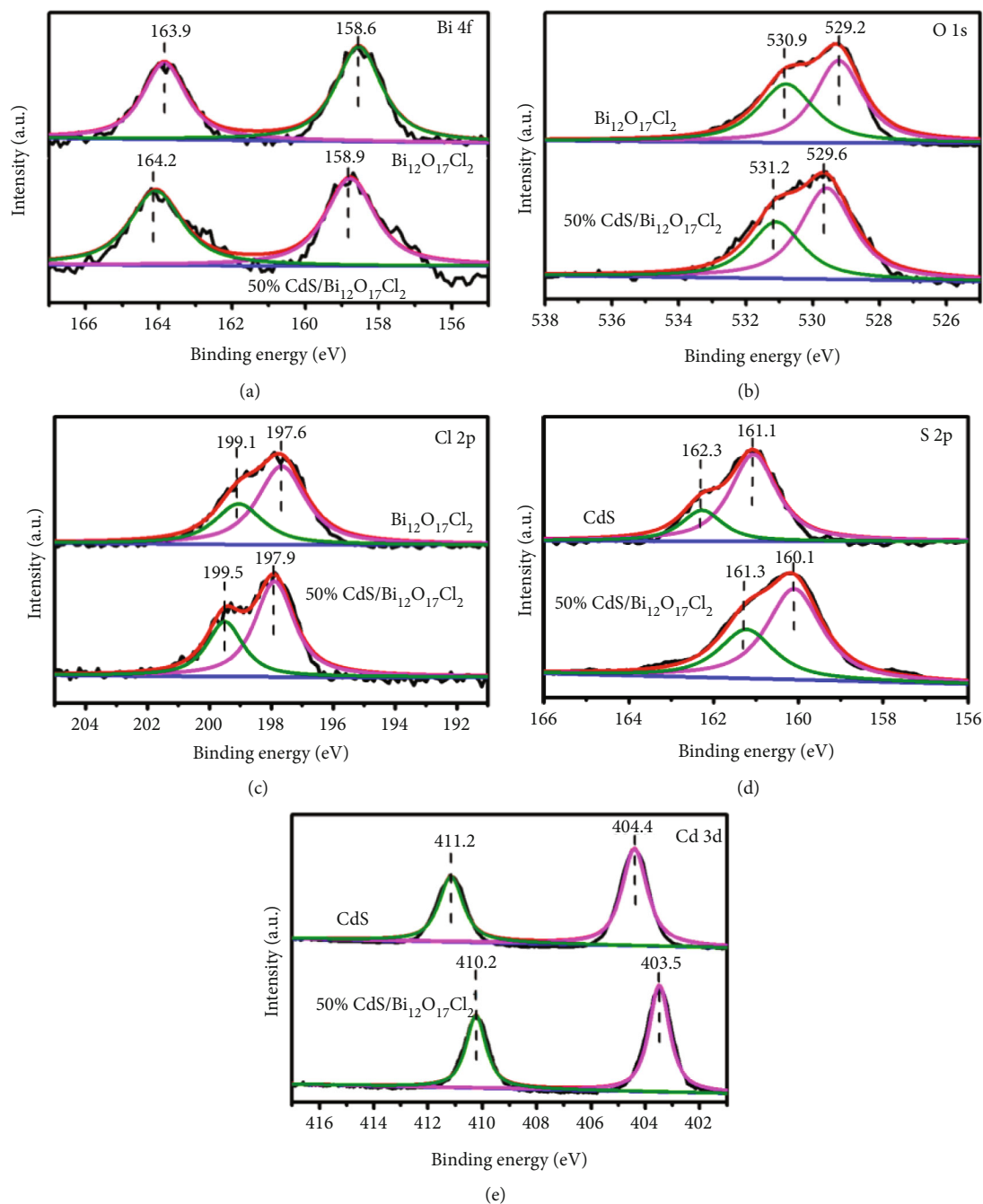


FIGURE 3: XPS spectra of Bi 4f (a), O 1s (b), Cl 2p (c), S 2p (d), and Cd 3d (e).

changing the dosage of CdS, a series of CdS/Bi₁₂O₁₇Cl₂ samples were prepared. According to the mass content of cadmium sulfide, the samples were named as 34% CdS/Bi₁₂O₁₇Cl₂, 50% CdS/Bi₁₂O₁₇Cl₂, and 60% CdS/Bi₁₂O₁₇Cl₂, respectively.

2.2. Characterizations. X-ray diffraction (XRD) patterns were recorded by a Bruker D8 X-ray diffractometer with a Cu K α radiation source. X-ray photoelectron spectroscopy (XPS) and valence XPS spectra were carried out on a photoelectron spectrometer (VG ESCALAB 210). The microstructure was analyzed by transmission electron microscopy

(TEM, JEM-2100F) and high-resolution transmission electron microscopy (HRTEM, JEM-2100F). Ultraviolet-visible (UV-vis) absorption spectra were collected with a UV-vis spectrophotometer (TU-1901). The specific surface areas were measured on a Micromeritics 3Flex apparatus by nitrogen adsorption-desorption isotherms at 77 K.

2.3. Photoelectrochemical Test. An electrochemical workstation (CHI660C) with a three-electrode system was used to examine the photoelectrochemical properties under visible light irradiation. Platinum was chosen as the counter electrode, the saturated calomel electrode was used as the

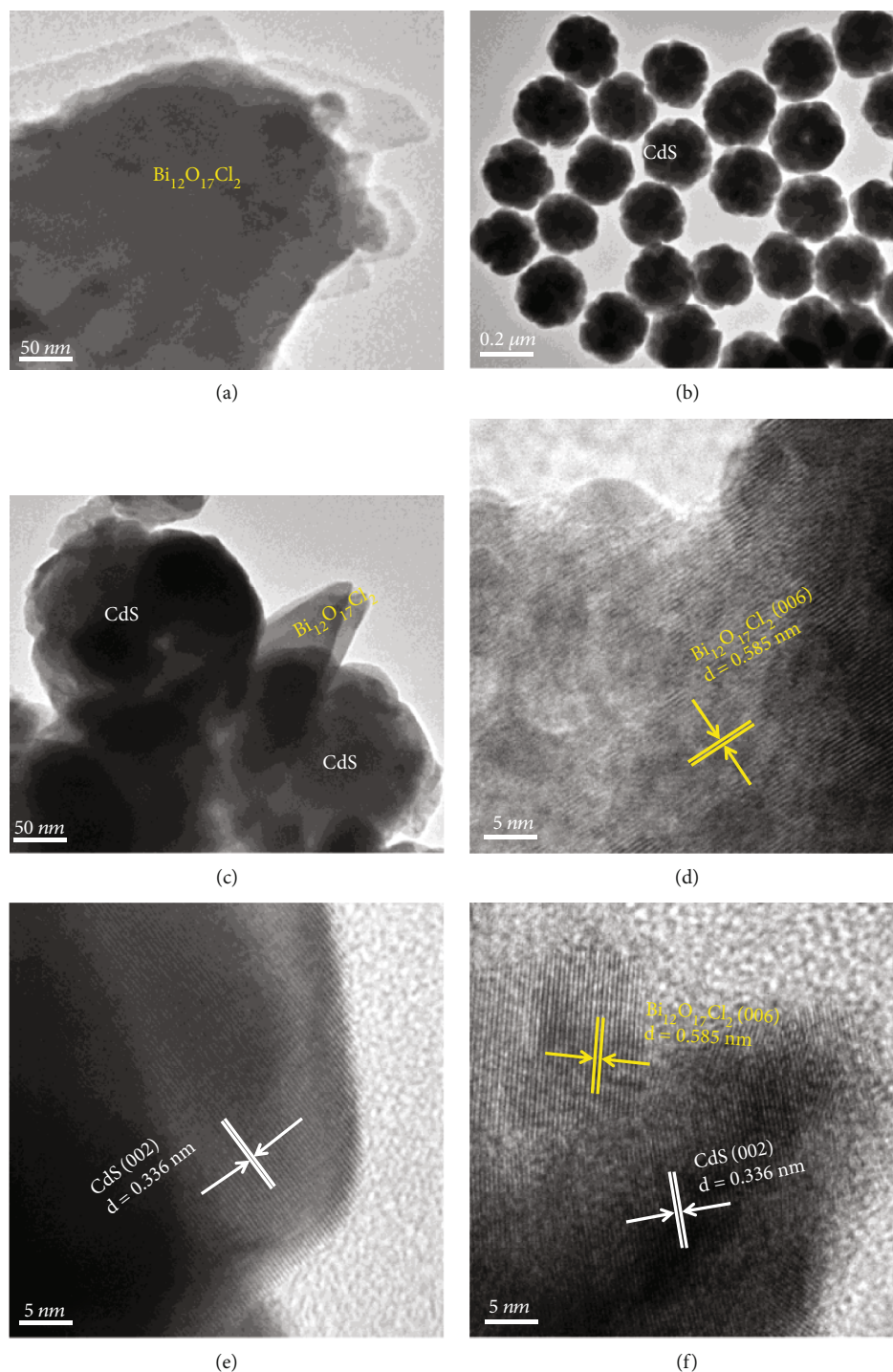


FIGURE 4: TEM and HRTEM images of $\text{Bi}_{12}\text{O}_{17}\text{Cl}_2$, CdS, and 50% CdS/ $\text{Bi}_{12}\text{O}_{17}\text{Cl}_2$.

reference electrode, and the working electrode was the thin film formed by coating the sample on ITO glasses. 5 mg sample was ultrasonically dispersed in N, N-dimethylformamide, and the mixture was then uniformly applied to ITO glass with an area of approximately 1 cm^2 and dried. The working electrode was ready to be completed. A 300 W Xe lamp was chosen as the light source, and Na_2SO_4 solution ($0.1\text{ mol}\cdot\text{L}^{-1}$) was selected for ion transport.

2.4. Photocatalytic Performance Measurements. The photocatalytic CO_2 reduction was carried out in an air-closed reactor (100 mL), which is equipped with a quartz window and two side sampling ports. A 300 W xenon lamp ($\lambda > 420\text{ nm}$) was chosen as the light source. High-purity CO_2 was pumped into the reactor for 30 minutes to remove O_2 . The sample (20 mg) with a Pt load of 0.5 wt% was scattered on a 4 cm^2 glass substrate. Then, the glass containing

samples was placed into the reactor. Ultrapure water (0.2 mL) was injected into the reaction system. Gas product from the reactor was fed into a gas chromatograph (GC-7890A, Agilent) at an interval of 1 h. The gas phase product was firstly separated in a carbon molecular sieve TDX-01 column and then entered the flame ionization detector to detect the content of methane. Qualitative analysis was carried out according to the retention time of the peak on the chromatographic outflow curve, and quantitative analysis was carried out according to the area of the peak.

The photocatalytic conversion of phenol was evaluated under the irradiation of a 300 W Xe lamp ($\lambda > 420$ nm). Firstly, catalysts with mass of 50 mg and $10 \text{ mg}\cdot\text{L}^{-1}$ phenol solution were stirred in the dark for 0.5 h. The light source was then turned on, and 5 mL of the reaction solution was taken every 15 minutes for analysis. A UV-vis spectrophotometer (TU-1901) was then used to determine the concentration of phenol solution.

3. Results and Discussion

3.1. Characterization Analysis. The phase composition of $\text{Bi}_{12}\text{O}_{17}\text{Cl}_2$, CdS, and $50\% \text{ CdS}/\text{Bi}_{12}\text{O}_{17}\text{Cl}_2$ samples was characterized by XRD (Figure 2). All diffraction peaks shown in Figures 2(a) and 2(e) were well matched with those of tetragonal $\text{Bi}_{12}\text{O}_{17}\text{Cl}_2$ (JCPDS No. 37-0702) [39] and CdS (JCPDS No. 77-2306) [38], respectively. Noticeably, no phase changes of CdS and $\text{Bi}_{12}\text{O}_{17}\text{Cl}_2$ and no indication of any new phase generation were observed after a thermal annealing procedure. For $50\% \text{ CdS}/\text{Bi}_{12}\text{O}_{17}\text{Cl}_2$, peaks corresponding to (100), (002), (101), (110), and (112) facets of CdS are clearly shown in Figure 2, and the peak intensity increased gradually with the increase of CdS content. However, the peak strength of (103) facet was very weak.

The surface chemical composition of $\text{Bi}_{12}\text{O}_{17}\text{Cl}_2$, CdS, and $50\% \text{ CdS}/\text{Bi}_{12}\text{O}_{17}\text{Cl}_2$ samples was measured by XPS. The binding energies of Bi 4f (Figure 3(a)) of the $50\% \text{ CdS}/\text{Bi}_{12}\text{O}_{17}\text{Cl}_2$ (158.9 and 164.2 eV) were shifted slightly to high value than those of pure $\text{Bi}_{12}\text{O}_{17}\text{Cl}_2$ (158.6 and 163.9 eV) [39]. For pure $\text{Bi}_{12}\text{O}_{17}\text{Cl}_2$, the XPS spectrum of O 1s (Figure 3(b)) could be divided into two peaks with binding energies of 529.2 eV and 530.9 eV, corresponding to the Bi-O bond and the O-H bond of H_2O that was adsorbed on the surface, respectively [37]. And the binding energy of O 1s XPS spectrum in the $50\% \text{ CdS}/\text{Bi}_{12}\text{O}_{17}\text{Cl}_2$ sample (529.6 and 531.2 eV) was higher than that in pure $\text{Bi}_{12}\text{O}_{17}\text{Cl}_2$. Furthermore, the binding energies of Cl 2p (197.9 and 199.5 eV) for the $50\% \text{ CdS}/\text{Bi}_{12}\text{O}_{17}\text{Cl}_2$ sample (Figure 3(c)) were shifted slightly to high value than those of pure $\text{Bi}_{12}\text{O}_{17}\text{Cl}_2$ (197.6 and 199.1 eV) [40]. For pure CdS, the binding energies of S 2p (Figure 3(d)) were 161.1 and 162.3 eV, and the binding energies of Cd 3d (Figure 3(e)) were 404.4 and 411.2 eV [41]. In the $50\% \text{ CdS}/\text{Bi}_{12}\text{O}_{17}\text{Cl}_2$ sample, the binding energies of S 2p (160.1 and 161.3 eV) and Cd 3d (403.5 and 410.2 eV) were shifted to a lower level. The shift of binding energy is resultant from the strong interaction between $\text{Bi}_{12}\text{O}_{17}\text{Cl}_2$ and CdS [42, 43], which is in accordance with the HRTEM results as discussed below.

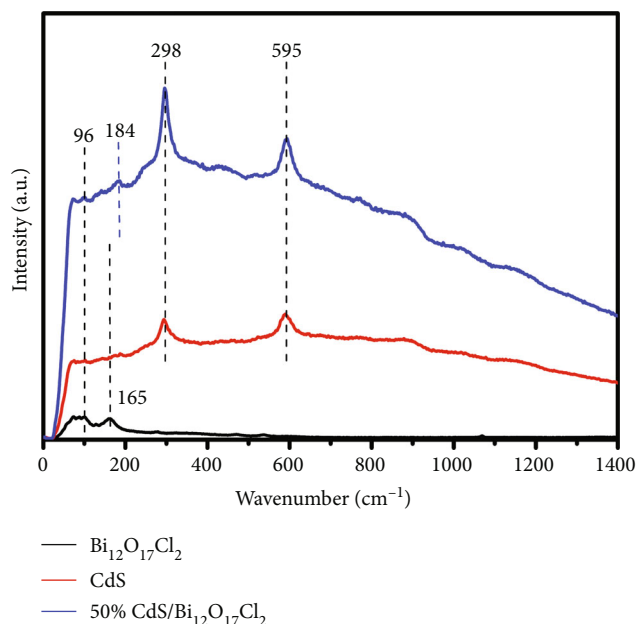


FIGURE 5: The Raman spectra of $\text{Bi}_{12}\text{O}_{17}\text{Cl}_2$, CdS and $50\% \text{ CdS}/\text{Bi}_{12}\text{O}_{17}\text{Cl}_2$.

The intimate contact between CdS and $\text{Bi}_{12}\text{O}_{17}\text{Cl}_2$ component is highly essential for charge transfer across the interfaces of $50\% \text{ CdS}/\text{Bi}_{12}\text{O}_{17}\text{Cl}_2$. TEM and HRTEM were carried out to visualize such contact in the samples. Figures 4(a)–4(c) showed the TEM image of $\text{Bi}_{12}\text{O}_{17}\text{Cl}_2$, CdS, and $50\% \text{ CdS}/\text{Bi}_{12}\text{O}_{17}\text{Cl}_2$, respectively. It can be observed that $\text{Bi}_{12}\text{O}_{17}\text{Cl}_2$ was an irregular block-shaped structure accumulated by nanometer slices (Figure 4(a)). In contrast, the CdS particles thus obtained were of typical microspheres with a diameter of ~ 250 nm (Figure 4(b)). HRTEM image in Figure 4(f) illustrated the clear lattice streaks, the spacing of 0.585 nm corresponded to (006) facet of $\text{Bi}_{12}\text{O}_{17}\text{Cl}_2$, and the spacing of 0.336 nm corresponded to (002) facet of CdS [23, 38]. This result was well consistent with the HRTEM results of pristine $\text{Bi}_{12}\text{O}_{17}\text{Cl}_2$ (Figure 4(d)) and CdS (Figure 4(e)). Thus, a heterogeneous interface was formed between CdS and $\text{Bi}_{12}\text{O}_{17}\text{Cl}_2$ which was conducive to charge transfer.

The Raman spectra were measured to research the chemical bonding information of $\text{Bi}_{12}\text{O}_{17}\text{Cl}_2$, CdS, and $50\% \text{ CdS}/\text{Bi}_{12}\text{O}_{17}\text{Cl}_2$ (Figure 5). For the $\text{Bi}_{12}\text{O}_{17}\text{Cl}_2$ phase, the bands situated at about 96 and 165 cm^{-1} could be attributed to the A_{1g} and E_g modes of external Bi-Cl stretching patterns [43]. For the CdS phase, two peaks at 298 and 595 cm^{-1} were attributed to the first-order and second-order longitudinal optical modes, respectively [44]. In the pattern of $50\% \text{ CdS}/\text{Bi}_{12}\text{O}_{17}\text{Cl}_2$, both the characteristic peaks of $\text{Bi}_{12}\text{O}_{17}\text{Cl}_2$ and CdS could be observed. In addition, the peak at 165 cm^{-1} was obviously shifted to the right, indicating that CdS affected the Bi-Cl stretching patterns of $\text{Bi}_{12}\text{O}_{17}\text{Cl}_2$, which could prove the existence of bonds between CdS and $\text{Bi}_{12}\text{O}_{17}\text{Cl}_2$ [37].

3.2. Light Absorption and Band Structure Analysis. Figure 6 shows the light absorption patterns and bandgap energies

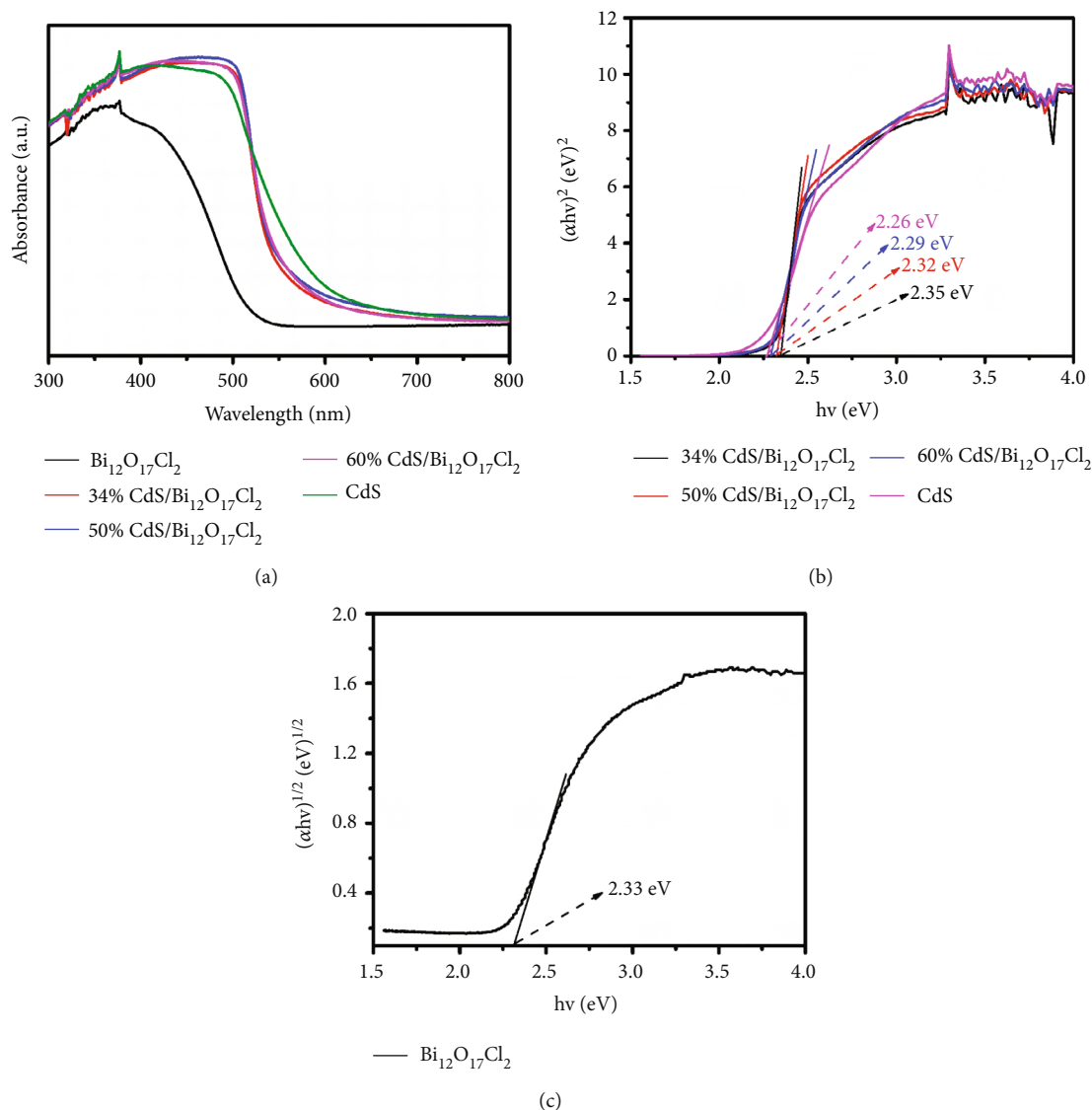


FIGURE 6: UV-vis absorption patterns (a) and bandgap energies (b, c) of Bi₁₂O₁₇Cl₂, 34% CdS/Bi₁₂O₁₇Cl₂, 50% CdS/Bi₁₂O₁₇Cl₂, 60% CdS/Bi₁₂O₁₇Cl₂, and CdS.

of the samples. The UV-vis absorption spectra (Figure 6(a)) of CdS/Bi₁₂O₁₇Cl₂ heterostructures mainly exhibited the absorption feature of CdS owing to the relatively high content (34%-60%) of CdS in the heterostructures. Interestingly, CdS/Bi₁₂O₁₇Cl₂ heterostructures showed an absorption edge at ~550 nm, although the CdS content in CdS/Bi₁₂O₁₇Cl₂ heterostructures increased. This result indicated that the light would be mainly absorbed by CdS during the photocatalytic reactions. The bandgap energies of these samples were calculated following the formula

$$\alpha h\nu = A(h\nu - E_g)^{n/2}, \quad (1)$$

where α , h , ν , E_g , and A represent the light absorption coefficient, Planck constant, frequency, bandgap energy, and constant, respectively [45]. Bi₁₂O₁₇Cl₂ is an indirect bandgap semiconductor, while CdS belongs to direct bandgap semicon-

ductors, so their n values are 4 and 1, respectively [46–48]. As shown in Figures 6(b) and 6(c), the bandgaps of CdS, 60% CdS/Bi₁₂O₁₇Cl₂, 50% CdS/Bi₁₂O₁₇Cl₂, 34% CdS/Bi₁₂O₁₇Cl₂, and Bi₁₂O₁₇Cl₂ were 2.26, 2.29, 2.32, 2.35, and 2.33 eV, respectively.

3.3. BET-BJH. The N₂ adsorption-desorption isotherms and pore size distribution of all samples are shown in Figure 7. The specific surface areas were measured to be 4, 20, 13, 22, and 16 m²·g⁻¹, and the pore sizes were 11.7, 3.8, 14.6, 16.1, and 16.0 nm for Bi₁₂O₁₇Cl₂, CdS, 34% CdS/Bi₁₂O₁₇Cl₂, 50% CdS/Bi₁₂O₁₇Cl₂, and 60% CdS/Bi₁₂O₁₇Cl₂, respectively. It can be observed that the specific surface area and pore size of CdS/Bi₁₂O₁₇Cl₂ samples increased at first and then decreased with the increase of CdS content.

3.4. Photocatalytic Activity and Stability. We compared the photocatalytic CO₂ reduction activity of samples under

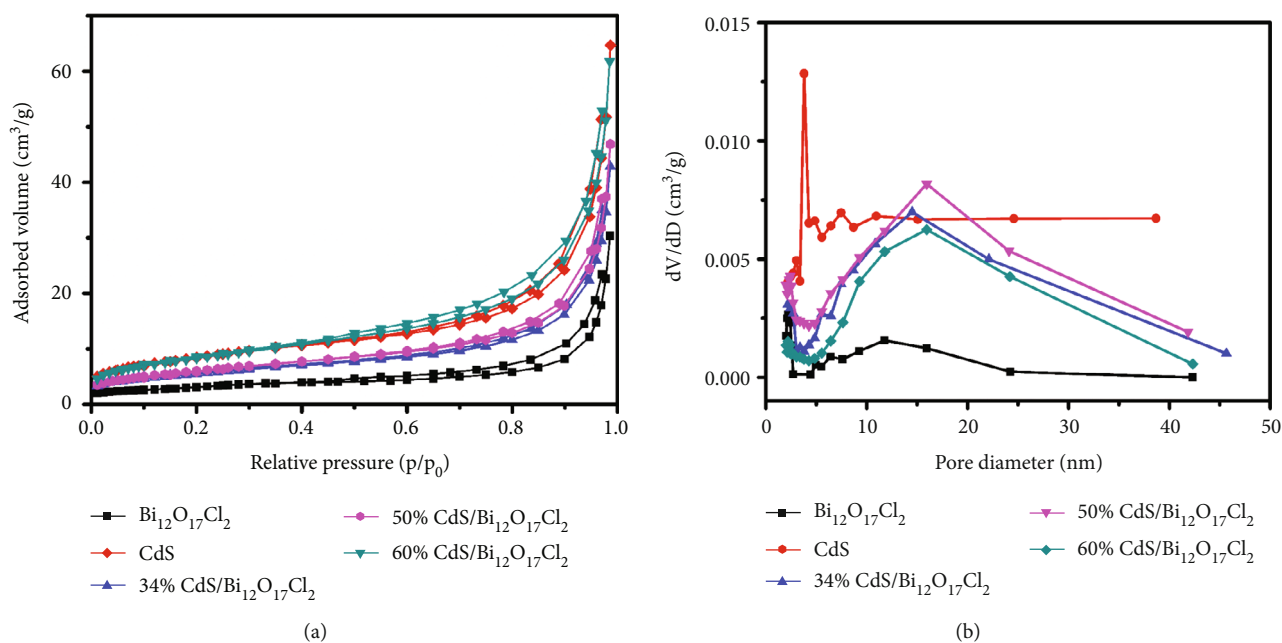


FIGURE 7: N₂ adsorption-desorption isotherms and pore size distribution of Bi₁₂O₁₇Cl₂, CdS, 34% CdS/Bi₁₂O₁₇Cl₂, 50% CdS/Bi₁₂O₁₇Cl₂, and 60% CdS/Bi₁₂O₁₇Cl₂.

visible light exposure, revealing the contribution of the CdS/Bi₁₂O₁₇Cl₂ heterojunction (Figure 8). Bi₁₂O₁₇Cl₂ and CdS offered a very low activity for CH₄ generation, with a rate of 0.13 and 0.22 $\mu\text{mol}\cdot\text{h}^{-1}\cdot\text{g}^{-1}$, respectively. Very encouraging, CdS/Bi₁₂O₁₇Cl₂ heterojunctions resulted in a highly increased performance for CH₄ generation. The CH₄ generation rate for 34% CdS/Bi₁₂O₁₇Cl₂ (0.65 $\mu\text{mol}\cdot\text{h}^{-1}\cdot\text{g}^{-1}$) was as 5.0 and 3.0 times as the CH₄ generation rate of pristine Bi₁₂O₁₇Cl₂ and CdS, respectively. The highest CH₄ generation rate was 1.28 $\mu\text{mol}\cdot\text{h}^{-1}\cdot\text{g}^{-1}$ on the 50% CdS/Bi₁₂O₁₇Cl₂ sample. In comparison, a physical mixture of CdS and Bi₁₂O₁₇Cl₂ with a mass ratio of 1 : 1 only had a CH₄ generation rate of 0.29 $\mu\text{mol}\cdot\text{h}^{-1}\cdot\text{g}^{-1}$. The above results validated that 50% CdS/Bi₁₂O₁₇Cl₂ heterostructure could efficiently separate the photon-generated carriers in CdS and Bi₁₂O₁₇Cl₂ and thus lead to enhanced CH₄ generation. Further increasing of CdS content led to a decreased CH₄ generation rate of 1.02 $\mu\text{mol}\cdot\text{h}^{-1}\cdot\text{g}^{-1}$ (60% CdS/Bi₁₂O₁₇Cl₂). The photocatalytic performance of CdS was better than that of Bi₁₂O₁₇Cl₂, which may be due to the larger specific surface area, better visible light absorption performance, and smaller bandgaps of CdS than Bi₁₂O₁₇Cl₂.

Furthermore, we tested the photocatalytic conversion of phenol on CdS/Bi₁₂O₁₇Cl₂ samples since the band energy positions of CdS and Bi₁₂O₁₇Cl₂ were suitable for oxidation reactions as discussed below. As shown in Figure 9, phenol was hard to be converted under visible light irradiation as exemplified by the blank experiment. After 2.5 h photocatalytic reaction, the conversion ratios of phenol for Bi₁₂O₁₇Cl₂, CdS, 34% CdS/Bi₁₂O₁₇Cl₂, 50% CdS/Bi₁₂O₁₇Cl₂, 60% CdS/Bi₁₂O₁₇Cl₂, and mechanical mixing 50% CdS/Bi₁₂O₁₇Cl₂ were about 41%, 48%, 69%, 92%, 81%, and 59%, respectively. Also, Bi₁₂O₁₇Cl₂ and CdS exhibited weak activity for phenol conversion, as occurred for CH₄ generation. However, upon

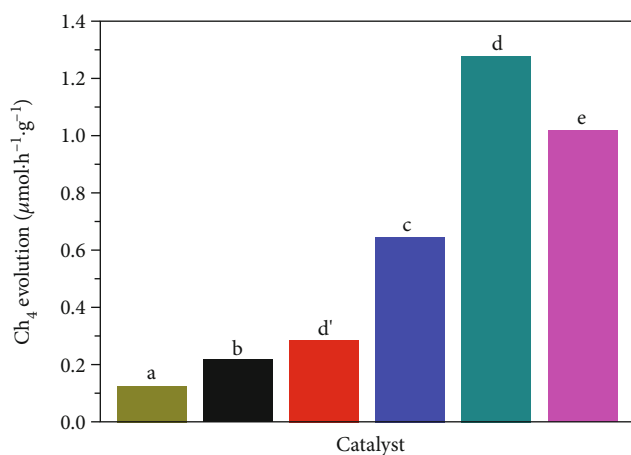


FIGURE 8: Yields of CH₄ for Bi₁₂O₁₇Cl₂ (a), CdS (b), 34% CdS/Bi₁₂O₁₇Cl₂ (c), 50% CdS/Bi₁₂O₁₇Cl₂ (d), 60% CdS/Bi₁₂O₁₇Cl₂ (e), and mechanical mixing 50% CdS/Bi₁₂O₁₇Cl₂ (d') under visible light irradiation ($\lambda > 420$ nm).

coupling CdS with Bi₁₂O₁₇Cl₂, an evidently increased rate for phenol conversion was realized. Phenol could be almost totally converted on 50% CdS/Bi₁₂O₁₇Cl₂ heterostructure in less than 3 hours. By contrast, the simple mixture of CdS and Bi₁₂O₁₇Cl₂ at this weight ratio only converted about 59% phenol under the same condition. As shown in Figure 10, the photodegradation process was consistent with the pseudo-first-order kinetic model, as expressed by the following equation:

$$-\ln\left(\frac{C}{C_0}\right) = kt, \quad (2)$$

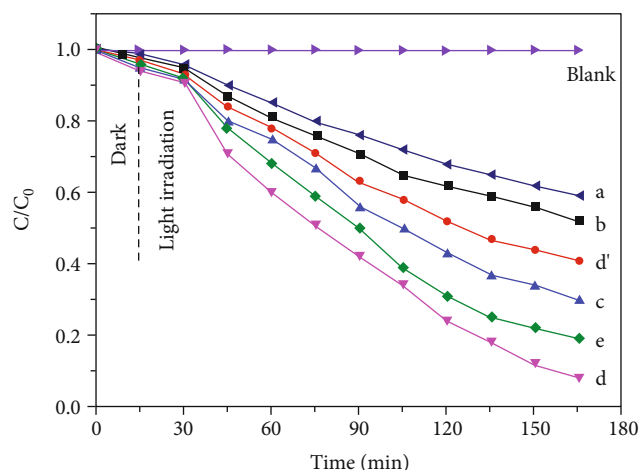


FIGURE 9: Phenol conversion of $\text{Bi}_{12}\text{O}_{17}\text{Cl}_2$ (a), CdS (b), 34% CdS/ $\text{Bi}_{12}\text{O}_{17}\text{Cl}_2$ (c), 50% CdS/ $\text{Bi}_{12}\text{O}_{17}\text{Cl}_2$ (d), 60% CdS/ $\text{Bi}_{12}\text{O}_{17}\text{Cl}_2$ (e), and mechanical mixing 50% CdS/ $\text{Bi}_{12}\text{O}_{17}\text{Cl}_2$ (d') under visible light irradiation ($\lambda > 420$ nm).

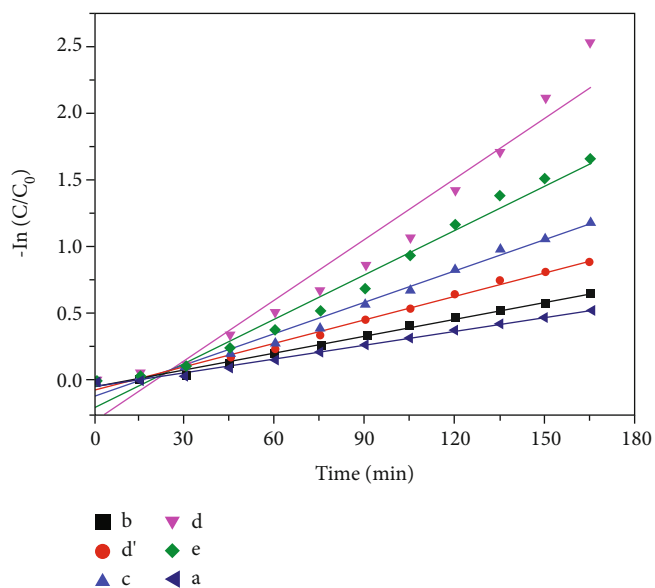


FIGURE 10: The conversion ratio constants under the pseudo-first-order kinetics model of $\text{Bi}_{12}\text{O}_{17}\text{Cl}_2$ (a), CdS (b), 34% CdS/ $\text{Bi}_{12}\text{O}_{17}\text{Cl}_2$ (c), 50% CdS/ $\text{Bi}_{12}\text{O}_{17}\text{Cl}_2$ (d), 60% CdS/ $\text{Bi}_{12}\text{O}_{17}\text{Cl}_2$ (e), and mechanical mixing 50% CdS/ $\text{Bi}_{12}\text{O}_{17}\text{Cl}_2$ (d').

where k represents the apparent rate constant calculated from the pseudo-first-order reaction kinetics model and C and C_0 are the concentration at time of t and zero, respectively [33]. As shown in Figure 10, the apparent rate constants for $\text{Bi}_{12}\text{O}_{17}\text{Cl}_2$, CdS, 34% CdS/ $\text{Bi}_{12}\text{O}_{17}\text{Cl}_2$, 50% CdS/ $\text{Bi}_{12}\text{O}_{17}\text{Cl}_2$, 60% CdS/ $\text{Bi}_{12}\text{O}_{17}\text{Cl}_2$, and mechanical mixing 50% CdS/ $\text{Bi}_{12}\text{O}_{17}\text{Cl}_2$ were 0.0036, 0.0043, 0.0078, 0.0151, 0.0116, and 0.0059 min^{-1} , respectively. Obviously, 50% CdS/ $\text{Bi}_{12}\text{O}_{17}\text{Cl}_2$ revealed the highest photocatalytic activity for phenol conversion. In addition, the removal ratio of chemical oxygen demand (COD) of phenol solution ($10 \text{ mg}\cdot\text{L}^{-1}$, 50 mL) with 50 mg 50% CdS/ $\text{Bi}_{12}\text{O}_{17}\text{Cl}_2$ reached

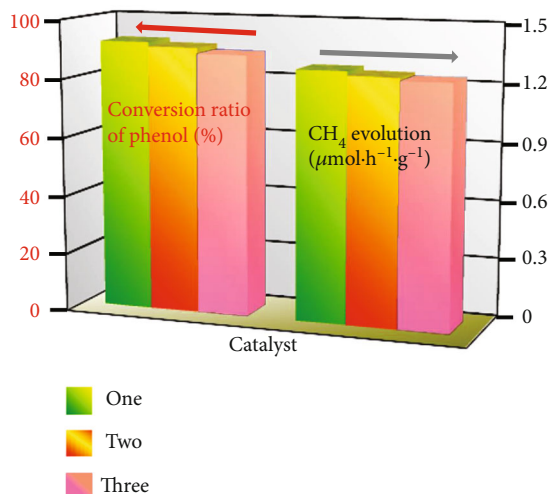


FIGURE 11: Stability test of phenol conversion and CH_4 evolution for 50% CdS/ $\text{Bi}_{12}\text{O}_{17}\text{Cl}_2$ recycling three times under visible light irradiation ($\lambda > 420$ nm).

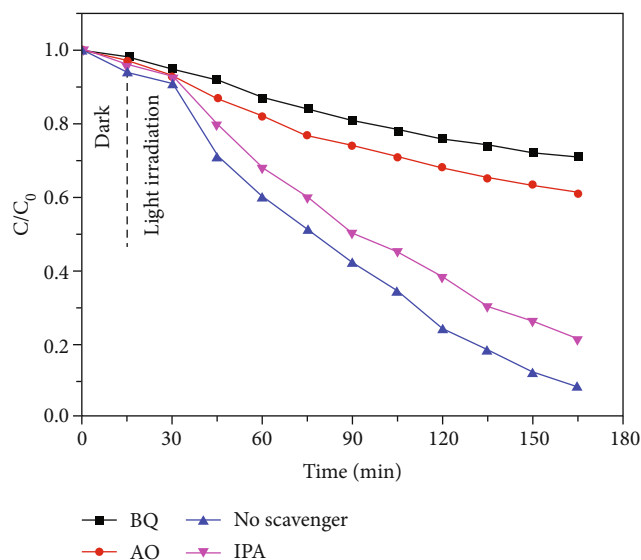


FIGURE 12: Effects of scavengers for phenol conversion in the 50% CdS/ $\text{Bi}_{12}\text{O}_{17}\text{Cl}_2$ photocatalytic system under visible light irradiation ($\lambda > 420$ nm).

30% after 4 h illumination (a 300 W xenon lamp was used as the light source).

The above results clearly demonstrated that the thermal annealing could ensure activity for phenol conversion. Moreover, 50% CdS/ $\text{Bi}_{12}\text{O}_{17}\text{Cl}_2$ heterostructure exhibited the highly stable activity for both CH_4 generation and phenol conversion. Only little change was observed on the reaction rates for CH_4 generation and phenol conversion in three consecutive experiments, as shown in Figure 11, illustrating the excellent durability of 50% CdS/ $\text{Bi}_{12}\text{O}_{17}\text{Cl}_2$ for long-term reaction.

3.5. Photocatalytic Mechanism Analysis. The active substances for the conversion of phenol on CdS/ $\text{Bi}_{12}\text{O}_{17}\text{Cl}_2$

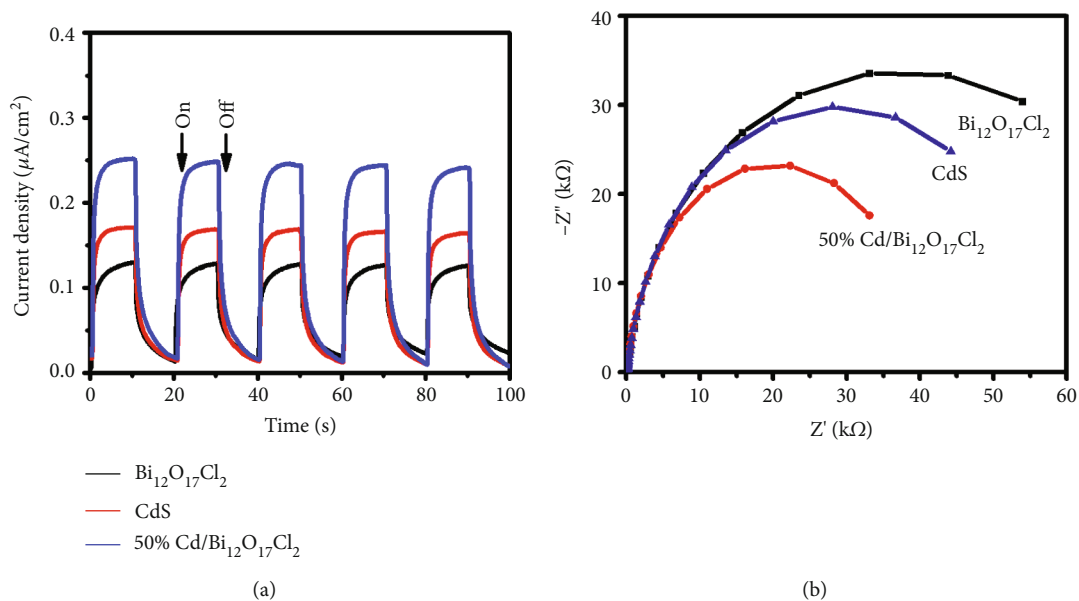


FIGURE 13: Transient photocurrent responses (a) and EIS Nyquist plots (b) of $\text{Bi}_{12}\text{O}_{17}\text{Cl}_2$, 50% $\text{CdS}/\text{Bi}_{12}\text{O}_{17}\text{Cl}_2$, and CdS .

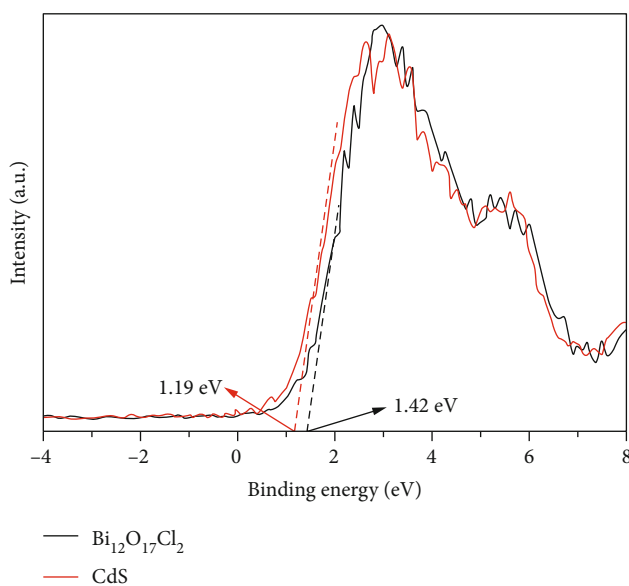


FIGURE 14: XPS valence spectra of $\text{Bi}_{12}\text{O}_{17}\text{Cl}_2$ and CdS .

were studied by free radical capture experiments, in which ammonium oxalate monohydrate (AO) was selected as the trapping agent for holes, isopropanol (IPA) for $\cdot\text{OH}$, and benzoquinone (BQ) for $\cdot\text{O}_2^-$, respectively. As illustrated in Figure 12, the addition of BQ and AO could greatly hinder the phenol conversion under visible light exposure, indicating that $\cdot\text{O}_2^-$ and h^+ are two prime active substances for phenol conversion. In comparison, only a slight decrease of phenol conversion occurred when IPA was added to the reaction suspension, thereby excluding $\cdot\text{OH}$ as the active substance in present case.

The increased photocatalytic activity for CH_4 generation and phenol conversion could be attributed to the enhanced interfacial charge transfer between CdS and $\text{Bi}_{12}\text{O}_{17}\text{Cl}_2$. This

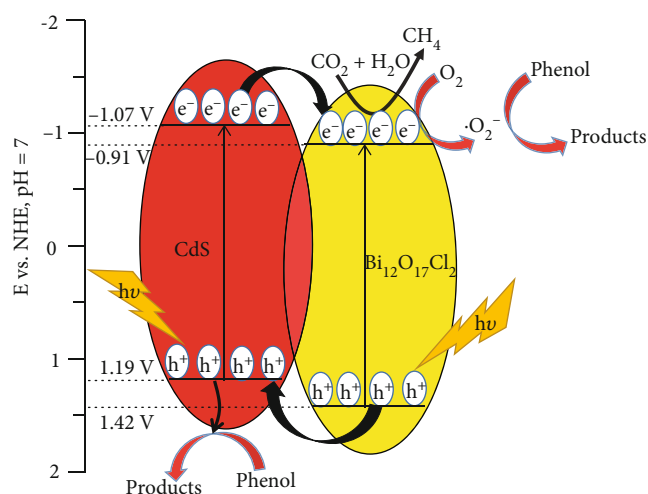


FIGURE 15: Proposed photocatalytic conversion mechanism of $\text{CdS}/\text{Bi}_{12}\text{O}_{17}\text{Cl}_2$ heterojunction under visible light irradiation ($\lambda > 420 \text{ nm}$).

efficient charge separation was verified by the photoelectrochemical tests. As illustrated in Figure 13(a), the 50% $\text{CdS}/\text{Bi}_{12}\text{O}_{17}\text{Cl}_2$ sample provided the highest transient photocurrent compared to pristine CdS and $\text{Bi}_{12}\text{O}_{17}\text{Cl}_2$, in spite of relatively low value. In addition, the low interface impedance in the 50% $\text{CdS}/\text{Bi}_{12}\text{O}_{17}\text{Cl}_2$ sample was also favorable for charge transfer, as exemplified by the small arc radius shown in Figure 13(b).

The band energy positions for CdS and $\text{Bi}_{12}\text{O}_{17}\text{Cl}_2$ were determined by the XPS valence spectra. As shown in Figure 14, the maximum valence band (VB) value of $\text{Bi}_{12}\text{O}_{17}\text{Cl}_2$ was 1.42 eV, while that of CdS was 1.19 eV. The bandgaps of pristine $\text{Bi}_{12}\text{O}_{17}\text{Cl}_2$ and CdS were 2.33 and 2.26 eV, respectively. Therefore, the conduction band (CB)

minimum was -1.07 eV for CdS and it was -0.91 eV for $\text{Bi}_{12}\text{O}_{17}\text{Cl}_2$. The electrons in the VB are excited by light to transition to the CB, as shown in Figure 15. Since the CB of $\text{Bi}_{12}\text{O}_{17}\text{Cl}_2$ is lower than that of CdS, the photoexcited electrons of CdS would transfer to $\text{Bi}_{12}\text{O}_{17}\text{Cl}_2$, and the hole would transfer reversely, namely, from $\text{Bi}_{12}\text{O}_{17}\text{Cl}_2$ to CdS. Such charge transfer can efficiently separate the electron-hole pair, thus enhancing the photocatalytic property for CH_4 generation and phenol conversion. The electrons accumulated in $\text{Bi}_{12}\text{O}_{17}\text{Cl}_2$ would reduce CO_2 and H_2O to CH_4 . Meanwhile, photoexcited electrons can also react with oxygen to produce superoxide radical O_2^- . Superoxide radicals and holes have strong oxidation ability, which can convert phenol into small molecules such as H_2O and CO_2 .

4. Conclusions

In summary, the CdS/ $\text{Bi}_{12}\text{O}_{17}\text{Cl}_2$ heterojunction has been successfully synthesized by means of thermal annealing. The results of photocatalytic activity experiments showed that CdS/ $\text{Bi}_{12}\text{O}_{17}\text{Cl}_2$ heterojunctions could considerably improve the performance for CO_2 reduction to CH_4 and phenol conversion under visible light exposure. In addition, 50% CdS/ $\text{Bi}_{12}\text{O}_{17}\text{Cl}_2$ showed the highest photocatalytic activity with a CH_4 generation of $1.28\ \mu\text{mol}\cdot\text{h}^{-1}\cdot\text{g}^{-1}$ and phenol removal ratio of 92% after 2.5 h of light irradiation. The activity enhancement is resultant from the effective division of photogenerated electron-hole pairs across the CdS/ $\text{Bi}_{12}\text{O}_{17}\text{Cl}_2$ interfaces. The study offers a new insight on exploring effective heterostructure photocatalysts for fuel manufacture and organic pollutant conversion.

Data Availability

The data used to support the findings of this study are included within the article.

Conflicts of Interest

The authors declare that they have no known competing financial interests or personal relationships that could have appeared to influence the work reported in this paper.

Authors' Contributions

Dandan Hu and Yumin Cui contributed equally to this work.

Acknowledgments

Thanks are due to the support of National Natural Science Foundation in China (21807012), Natural Science Foundation of Anhui Province in China (gxgwx2018059, KJ2020ZD47), Key Research and Development Programs of Anhui Province in 2021 (202104i07020011), Natural Science Research Projects of Fuyang Normal University of China (2017FSKJ09), Horizontal Cooperation Project of Fuyang municipal government and Fuyang Normal University (XDHX2016002, XDHX201711, XDHXPT201702, and XDHX201716), Scientific Research Innovation Team of

Fuyang Normal University (kytd201707), and Innovative training program for College Students (201910371021, S201910371022, and S201910371022) in China. We would also like to thank the university engineering technology research center of biomass conversion and antipollution control of Anhui province platform for supporting this work.

References

- [1] S. F. An, G. H. Zhang, T. W. Wang et al., "High-density ultra-small clusters and single-atom Fe sites embedded in graphitic carbon nitride (g-C₃N₄) for highly efficient catalytic advanced oxidation processes," *ACS Nano*, vol. 12, no. 9, pp. 9441–9450, 2018.
- [2] X. Y. Shen, H. M. Shao, Y. Liu, and Y. C. Zhai, "Synthesis and photocatalytic performance of ZnO with flower-like structure from zinc oxide ore," *Journal of Materials Science and Technology*, vol. 51, pp. 1–7, 2020.
- [3] C. Gao, S. M. Chen, Y. Wang et al., "Heterogeneous single-atom catalyst for visible-light-driven high-turnover CO_2 reduction: the role of electron transfer," *Advanced Materials*, vol. 30, no. 13, article 1704624, 2018.
- [4] M. Hesari, X. W. Mao, and P. Chen, "Charge carrier activity on single-particle photo(electro)catalysts: toward function in solar energy conversion," *Journal of the American Chemical Society*, vol. 140, no. 22, pp. 6729–6740, 2018.
- [5] W. N. Shi, X. W. Guo, C. X. Cui et al., "Controllable synthesis of Cu_2O decorated WO_3 nanosheets with dominant (0 0 1) facets for photocatalytic CO_2 reduction under visible-light irradiation," *Applied Catalysis B: Environmental*, vol. 243, pp. 236–242, 2019.
- [6] X. L. Liu, S. Xu, H. B. Chi et al., "Ultrafine 1D graphene interlayer in g-C₃N₄/graphene/recycled carbon fiber heterostructure for enhanced photocatalytic hydrogen generation," *Chemical Engineering Journal*, vol. 359, pp. 1352–1359, 2019.
- [7] Y. F. Guo, J. Li, Y. P. Yuan et al., "A rapid microwave-assisted thermolysis route to highly crystalline carbon nitrides for efficient hydrogen generation," *Angewandte Chemie, International Edition*, vol. 55, no. 47, pp. 14693–14697, 2016.
- [8] N. X. Li, X. C. Liu, J. C. Zhou, W. S. Chen, and M. C. Liu, "Encapsulating CuO quantum dots in MIL-125(Ti) coupled with g-C₃N₄ for efficient photocatalytic CO_2 reduction," *Chemical Engineering Journal*, vol. 399, article 125782, 2020.
- [9] M. L. Li, L. X. Zhang, M. Y. Wu et al., "Mesoporous CeO_2 /g-C₃N₄ nanocomposites: Remarkably enhanced photocatalytic activity for CO_2 reduction by mutual component activations," *Nano Energy*, vol. 19, pp. 145–155, 2016.
- [10] G. P. Gao, Y. Jiao, E. R. Waclawik, and A. J. Du, "Single atom (Pd/Pt) supported on graphitic carbon nitride as an efficient photocatalyst for visible-light reduction of carbon dioxide," *Journal of the American Chemical Society*, vol. 138, no. 19, pp. 6292–6297, 2016.
- [11] W. Ma, N. Wang, Y. Guo et al., "Enhanced photoreduction CO_2 activity on g-C₃N₄: by synergistic effect of nitrogen defective-enriched and porous structure, and mechanism insights," *Chemical Engineering Journal*, vol. 388, article 124288, 2020.
- [12] Q. Chen, H. M. Long, M. J. Chen, Y. F. Rao, X. W. Li, and Y. Huang, "In situ construction of biocompatible Z-scheme $\alpha\text{-Bi}_2\text{O}_3/\text{CuBi}_2\text{O}_4$ heterojunction for NO removal under

- visible light,” *Applied Catalysis B: Environmental*, vol. 272, article 119008, 2020.
- [13] X. Y. Jin, Q. M. Guan, T. Tian et al., “In₂O₃/boron doped g-C₃N₄ heterojunction catalysts with remarkably enhanced visible-light photocatalytic efficiencies,” *Applied Surface Science*, vol. 504, article 144241, 2020.
- [14] D. R. Qin, Y. Xia, Q. Li, C. Yang, Y. M. Qin, and K. L. Lv, “One-pot calcination synthesis of Cd_{0.5}Zn_{0.5}S/g-C₃N₄ photocatalyst with a step-scheme heterojunction structure,” *Journal of Materials Science and Technology*, vol. 56, pp. 206–215, 2020.
- [15] N. X. Qian, X. Zhang, X. Sun et al., “A facile method to tune the crystal lattice/morphology/electronic state/photocatalytic performance of BiOCl,” *Journal of Alloys and Compounds*, vol. 815, article 152490, 2020.
- [16] S. B. Ning, L. Y. Ding, Z. G. Lin et al., “One-pot fabrication of Bi₃O₄Cl/BiOCl plate-on-plate heterojunction with enhanced visible-light photocatalytic activity,” *Applied Catalysis B: Environmental*, vol. 185, pp. 203–212, 2016.
- [17] X. Y. Xiao, J. Jiang, and L. Z. Zhang, “Selective oxidation of benzyl alcohol into benzaldehyde over semiconductors under visible light: The case of Bi₁₂O₁₇C₁₂ nanobelts,” *Applied Catalysis B: Environmental*, vol. 142–143, pp. 487–493, 2013.
- [18] G. Chen, G. L. Fang, and G. D. Tang, “Photoluminescence and photocatalytic properties of BiOCl and Bi₂₄O₃₁Cl₁₀ nanostructures synthesized by electrolytic corrosion of metal Bi,” *Materials Research Bulletin*, vol. 48, no. 3, pp. 1256–1261, 2013.
- [19] J. Di, C. Zhu, M. X. Ji et al., “Defect-rich Bi₁₂O₁₇C₁₂ nanotubes self-accelerating charge separation for boosting photocatalytic CO₂ reduction,” *Angewandte Chemie, International Edition*, vol. 57, no. 45, pp. 14847–14851, 2018.
- [20] C. J. Bi, J. Cao, H. L. Lin, Y. J. Wang, and S. F. Chen, “BiOI/Bi₁₂O₁₇C₁₂: a novel heterojunction composite with outstanding photocatalytic and photoelectric performances,” *Materials Letters*, vol. 166, pp. 267–270, 2016.
- [21] F. Chang, W. J. Yan, B. Lei et al., “In-situ constructing Bi₂S₃ nanocrystals-modified Bi₁₂O₁₇C₁₂ nanosheets with features of rich oxygen vacancies and reinforced photocatalytic performance,” *Separation and Purification Technology*, vol. 235, article 116171, 2020.
- [22] L. C. Tien, Y. L. Lin, and S. Y. Chen, “Synthesis and characterization of Bi₁₂O₁₇C₁₂ nanowires obtained by chlorination of α -Bi₂O₃ nanowires,” *Materials Letters*, vol. 113, pp. 30–33, 2013.
- [23] W. D. Zhang, X. A. Dong, B. Jia, J. B. Zhong, Y. J. Sun, and F. Dong, “2D BiOCl/Bi₁₂O₁₇Cl₂ nanojunction: Enhanced visible light photocatalytic NO removal and in situ DRIFTS investigation,” *Applied Surface Science*, vol. 430, pp. 571–577, 2018.
- [24] J. Y. Ma, L. Shi, Z. M. Wang, T. Q. Ren, Z. X. Geng, and W. Qi, “2D layered MoS₂ loaded on Bi₁₂O₁₇C₁₂ nanosheets: an effective visible-light photocatalyst,” *Ceramics International*, vol. 46, no. 6, pp. 7438–7445, 2020.
- [25] G. P. He, C. L. Xing, X. Xiao, R. P. Hu, X. X. Zuo, and J. M. Nan, “Facile synthesis of flower-like Bi₁₂O₁₇C₁₂/ β -Bi₂O₃ composites with enhanced visible light photocatalytic performance for the degradation of 4-tert-butylphenol,” *Applied Catalysis B: Environmental*, vol. 170–171, pp. 1–9, 2015.
- [26] H. J. Cui, Y. W. Zhou, J. F. Mei, Z. Y. Li, S. Xu, and C. Yao, “Synthesis of CdS/BiOBr nanosheets composites with efficient visible-light photocatalytic activity,” *Journal of Physics and Chemistry of Solids*, vol. 112, pp. 80–87, 2018.
- [27] S. Ma, Y. P. Deng, J. Xie et al., “Noble-metal-free Ni₃C cocatalysts decorated CdS nanosheets for high-efficiency visible-light-driven photocatalytic H₂ evolution,” *Applied Catalysis B: Environmental*, vol. 227, pp. 218–228, 2018.
- [28] Z. L. Wang, Y. F. Chen, L. Y. Zhang, B. Cheng, J. G. Yu, and J. J. Fan, “Step-scheme CdS/TiO₂ nanocomposite hollow microsphere with enhanced photocatalytic CO₂ reduction activity,” *Journal of Materials Science and Technology*, vol. 56, pp. 143–150, 2020.
- [29] Q. M. Sun, N. Wang, J. H. Yu, and J. C. Yu, “A hollow porous CdS photocatalyst,” *Advanced Materials*, vol. 30, no. 45, article 1804368, 2018.
- [30] Q. Liang, J. Jin, M. Zhang et al., “Construction of mesoporous carbon nitride/binary metal sulfide heterojunction photocatalysts for enhanced degradation of pollution under visible light,” *Applied Catalysis B: Environmental*, vol. 218, pp. 545–554, 2017.
- [31] H. J. Cui, B. B. Li, Z. Y. Li, X. Z. Li, and S. Xu, “Z-scheme based CdS/CdWO₄ heterojunction visible light photocatalyst for dye degradation and hydrogen evolution,” *Applied Surface Science*, vol. 455, pp. 831–840, 2018.
- [32] B. Chong, L. Chen, D. Z. Han et al., “CdS-modified one-dimensional g-C₃N₄ porous nanotubes for efficient visible-light photocatalytic conversion,” *Journal of Catalysis*, vol. 40, no. 6, pp. 959–968, 2019.
- [33] Q. Q. Li, W. L. Zhao, Z. C. Zhai, K. X. Ren, T. Y. Wang, and H. Guan, “2D/2D Bi₂MoO₆/g-C₃N₄ S-scheme heterojunction photocatalyst with enhanced visible-light activity by Au loading,” *Journal of Materials Science and Technology*, vol. 56, pp. 216–226, 2020.
- [34] T. P. Hu, K. Dai, J. F. Zhang, and S. F. Chen, “Noble-metal-free Ni₂P modified step-scheme SnNb₂O₆/CdS-diethylenetriamine for photocatalytic hydrogen production under broadband light irradiation,” *Applied Catalysis B: Environmental*, vol. 269, article 118844, 2020.
- [35] Z. Li, M. Chen, Q. W. Zhang, and D. P. Tao, “Mechanochemical synthesis of a Z-scheme Bi₂WO₆/CuBi₂O₄ heterojunction and its visible-light photocatalytic degradation of ciprofloxacin,” *Journal of Alloys and Compounds*, vol. 845, 2020.
- [36] S. L. Luan, D. Qu, L. An et al., “Enhancing photocatalytic performance by constructing ultrafine TiO₂ nanorods/g-C₃N₄ nanosheets heterojunction for water treatment,” *Science Bulletin*, vol. 63, no. 11, pp. 683–690, 2018.
- [37] J. J. Zheng, F. Chang, M. Z. Jiao, Q. Xu, B. Q. Deng, and X. F. Hu, “A visible-light-driven heterojunctioned composite WO₃/Bi₁₂O₁₇C₁₂: synthesis, characterization, and improved photocatalytic performance,” *Journal of Colloid and Interface Science*, vol. 510, pp. 20–31, 2018.
- [38] J. Wu, P. K. Liang, Q. W. Li et al., “Fabrication of CdS/BiOI heterostructure with enhanced photocatalytic performance under visible-light irradiation,” *Materials Letters*, vol. 218, pp. 5–9, 2018.
- [39] F. Chang, J. R. Luo, X. F. Wang, Y. C. Xie, B. Q. Deng, and X. F. Hu, “Poly(vinyl pyrrolidone)-assisted hydrothermal synthesis and enhanced visible-light photocatalytic performance of oxygen-rich bismuth oxychlorides,” *Journal of Colloid and Interface Science*, vol. 459, pp. 136–145, 2015.
- [40] W. D. Zhang, X. A. Dong, Y. Liang, Y. J. Sun, and F. Dong, “Ag/AgCl nanoparticles assembled on BiOCl/Bi₁₂O₁₇C₁₂ nanosheets: enhanced plasmonic visible light photocatalysis and in situ DRIFTS investigation,” *Applied Surface Science*, vol. 455, pp. 236–243, 2018.

- [41] S. S. Li, L. Wang, S. Liu et al., "In situ synthesis of strongly coupled Co_2P -CdS nanohybrids: an effective strategy to regulate photocatalytic hydrogen evolution activity," *Chemical Engineer*, vol. 6, no. 8, pp. 9940–9950, 2018.
- [42] N. Song, J. M. Li, C. M. Li et al., "In-situ fabrication of 0D/2D $\text{NiO}/\text{Bi}_{12}\text{O}_{17}\text{C}_{12}$ heterojunction towards high-efficiency degrading 2, 4-dichlorophenol and mechanism insight," *Journal of Photochemistry and Photobiology A: Chemistry*, vol. 386, 2020.
- [43] E. H. Jiang, L. Y. Yang, N. Song, X. X. Zhang, C. B. Liu, and H. J. Dong, "Multi-shelled hollow cube CaTiO_3 decorated with $\text{Bi}_{12}\text{O}_{17}\text{C}_{12}$ towards enhancing photocatalytic performance under the visible light," *Journal of Colloid and Interface Science*, vol. 576, pp. 21–33, 2020.
- [44] R. Shi, H. F. Ye, F. Liang et al., "Interstitial P-doped CdS with long-lived photogenerated electrons for photocatalytic water splitting without sacrificial agents," *Advanced Materials*, vol. 30, no. 6, article 1705941, 2018.
- [45] L. Hao, H. W. Huang, Y. X. Guo, X. Du, and Y. H. Zhang, "Bismuth oxychloride homogeneous phasejunction $\text{BiOCl}/\text{Bi}_{12}\text{O}_{17}\text{C}_{12}$ with unselectively efficient photocatalytic activity and mechanism insight," *Applied Surface Science*, vol. 420, pp. 303–312, 2017.
- [46] L. Wang, X. P. Min, X. Y. Sui, J. H. Chen, and Y. Wang, "Facile construction of novel $\text{BiOBr}/\text{Bi}_{12}\text{O}_{17}\text{C}_{12}$ heterojunction composites with enhanced photocatalytic performance," *Journal of Colloid and Interface Science*, vol. 560, pp. 21–33, 2020.
- [47] C. Y. Zhou, C. Lai, P. Xu et al., "ACS Sustainable," *Chemical Engineering*, vol. 6, no. 5, pp. 6941–6949, 2018.
- [48] Y. Y. Li, Z. H. Wei, J. B. Fan, Z. J. Li, and H. C. Yao, "Photocatalytic CO_2 reduction activity of Z-scheme CdS/CdWO_4 catalysts constructed by surface charge directed selective deposition of CdS," *Applied Surface Science*, vol. 483, pp. 442–452, 2019.